Inclusion complex vs. conjugation of hydrophobic photosensitizers with β-cyclodextrin: Improved disaggregation and photodynamic therapy efficacy against glioblastoma cells

Amina Ben Mihoub, Zahraa Youssef, Ludovic Colombeau, Valérie Jouan-Hureaux, Philippe Arnoux, Céline Frochot, Régis Vanderesse, Samir Acherar

Inclusion complex *vs.* conjugation of hydrophobic photosensitizers with β-cyclodextrin: Improved disaggregation and photodynamic therapy efficacy against glioblastoma cells

Amina Ben Mihoub,[a,b] *Zahraa Youssef,*[c] *Ludovic Colombeau,*[a,c] *Valérie Jouan-Hureaux,*[d] *Philippe Arnoux,*[c] *Céline Frochot,*[c] *Régis Vanderesse,*[a] *and Samir Acherar**[a]

[a] Université de Lorraine, CNRS, LCPM, F-54000 Nancy, France

[b] Laboratory of Physical Chemistry of Materials (LPCM), Faculty of Sciences, (UATL) BP 37G Laghouat 03000, Algeria

[c] Université de Lorraine, CNRS, LRGP, F-54000 Nancy, France

[d] Université de Lorraine, CNRS, CRAN, F-54000 Nancy, France

* Corresponding Author: samir.acherar@univ-lorraine.fr

Abstract

Self-aggregation of hydrophobic porphyrin-based photosensitizers (PSs) in aqueous biological environment decreases their bioavailability and *in vivo* therapeutic efficacy, which hampers their clinical use in photodynamic therapy (PDT). In the current study, we explore three new supramolecular systems based of hydrophobic PSs (*i.e.* 5,10,15,20-tetrakis(3-hydroxyphenyl)porphyrin (*m*THPP) or 5-(4-carboxyphenyl)-10,15,20-triphenylporphyrin (P1COOH)) non-covalently or covalently attached to β-CD. The two non-covalent solid inclusion complexes $(\beta\text{-CD})_2$/*m*THPP and $[(\beta\text{-CD})/\text{P1COOH}]_4$ are prepared by a new co-precipitation@lyophilization combined method and the covalent conjugate β-CD-P1 by click chemistry. The binding type effect and effectiveness on the disaggregation in aqueous medium and *in vitro* PDT efficacy against glioblastoma cancer cells of PSs are investigated for the three β-CD/PS systems. The findings reveal a remarkable improvement of the disaggregation and *in vitro* PDT activity of these β-CD/PS systems compared to the free PSs, except for $[(\beta\text{-CD})/\text{P1COOH}]_4$ inclusion complex

caused by J-type self-aggregation of the inclusion complex in tetrameric form. β-CD-P1 conjugate shows the higher *in vitro* PDT efficacy compared to the other β-CD/PS systems. Overall, the results indicate that the disaggregation in aqueous medium and *in vitro* PDT activity of hydrophobic PSs can be improved by their binding to β-CD and the covalent binding is the best approach.

Keywords: β-Cyclodextrin, Photosensitizer, Inclusion complex, Conjugation, Disaggregation, Photodynamic therapy, Glioblastoma.

Corresponding Author: E-mail: samir.acherar@univ-lorraine.fr. Phone: +33 037-274-3687**.**

1. Introduction

Photodynamic therapy (PDT) is a minimally invasive cancer treatment involving the generation of reactive oxygen species (ROS), particularly singlet oxygen ($^1O_2$), which causes cell apoptosis and necrosis [1]. ROS generation is based on the light photoactivation of a photosensitizer (PS) at a particular wavelength followed by its interaction with molecular oxygen. However, one of the major drawbacks of PDT is the poor water solubility of PSs, limiting their clinical usefulness. The most effective PSs for PDT are hydrophobic molecules which typically present a strong propensity to self-aggregate in water, resulting in lowered $^1O_2$ generation *(i.e* diminution of the PDT efficacy) and administration difficulties [2].

The emergence of the nanotechnology has deeply affected various biomedicine areas, including PDT [3]. Among the various branches of nanotechnology, the use of biocompatible nanovectors for PSs administration has paved the way for a significant improvement in their bioavailability, biodistribution and PDT efficacy [4-6]. Cyclodextrins (CDs) are by far one of the most promising biocompatible nanovectors of PSs [7,8] thanks to their water-soluble, biocompatible, crystalline and non-hygroscopic properties. CDs are a family of natural glucopyranose-based cyclic oligosaccharides, containing a relatively hydrophobic central cavity that can be used to form reversibly and selectively host-guest inclusion complexes with various guest molecules in aqueous media [9-14]. Inclusion complexation (non-covalent binding) or conjugation (covalent binding) of PSs with CDs lead to a significant improvement in water solubility, ROS production and PDT efficacy of PSs against cancer cells [15-19].

In this context, the present study aims to compare the effect and effectiveness of the binding type (non-covalent *vs.* covalent) of β-CD with hydrophobic PSs on the disaggregation in aqueous medium and *in vitro* PDT efficacy of PSs.

Our starting hypothesis is that a covalent link (β-CD–PS conjugate) must be more stable than non-covalent link (β-CD/PS inclusion complex) in aqueous medium because the complex formation and dissociation are dynamic equilibrium processes while the conjugate forms unbreakable covalent bond between β-CD and PS. Thus, we assume that the covalent link should give the better effect on PSs in terms of disaggregation in aqueous medium and *in vitro* PDT efficacy against glioblastoma cells.

To answer to the above hypothesis, we explore three new supramolecular systems based of hydrophobic PSs (*i.e.* 5,10,15,20-tetrakis(3-hydroxyphenyl)porphyrin (*m*THPP) or 5-(4-carboxyphenyl)-10,15,20-triphenylporphyrin (P1COOH)) non-covalently or covalently attached to β-CD. These supramolecular systems consist of two non-covalent solid inclusion complexes ((β-CD)$_2$/*m*THPP and [(β-CD)/P1COOH]$_4$) and one covalent conjugate (β-CD-P1) (Fig.1). The solid inclusion complexes are prepared by co-precipitation@lyophilization combined method and characterized by ^{1}H NMR, FTIR, XRD, TG-DTA techniques. The conjugate β-CD-P1 is synthesized using Copper-Catalyzed Azide-Alkyne Cycloaddition (CuAAC) click chemistry and characterized by NMR (^{1}H, ^{13}C, 2D HSQC and 2D HMBC) and HRMS techniques. The binding type effect and effectiveness of the β-CD/PS systems on the disaggregation in aqueous medium and *in vitro* PDT activity against glioblastoma U87 and U251 cells cancer cells are investigated and compared.

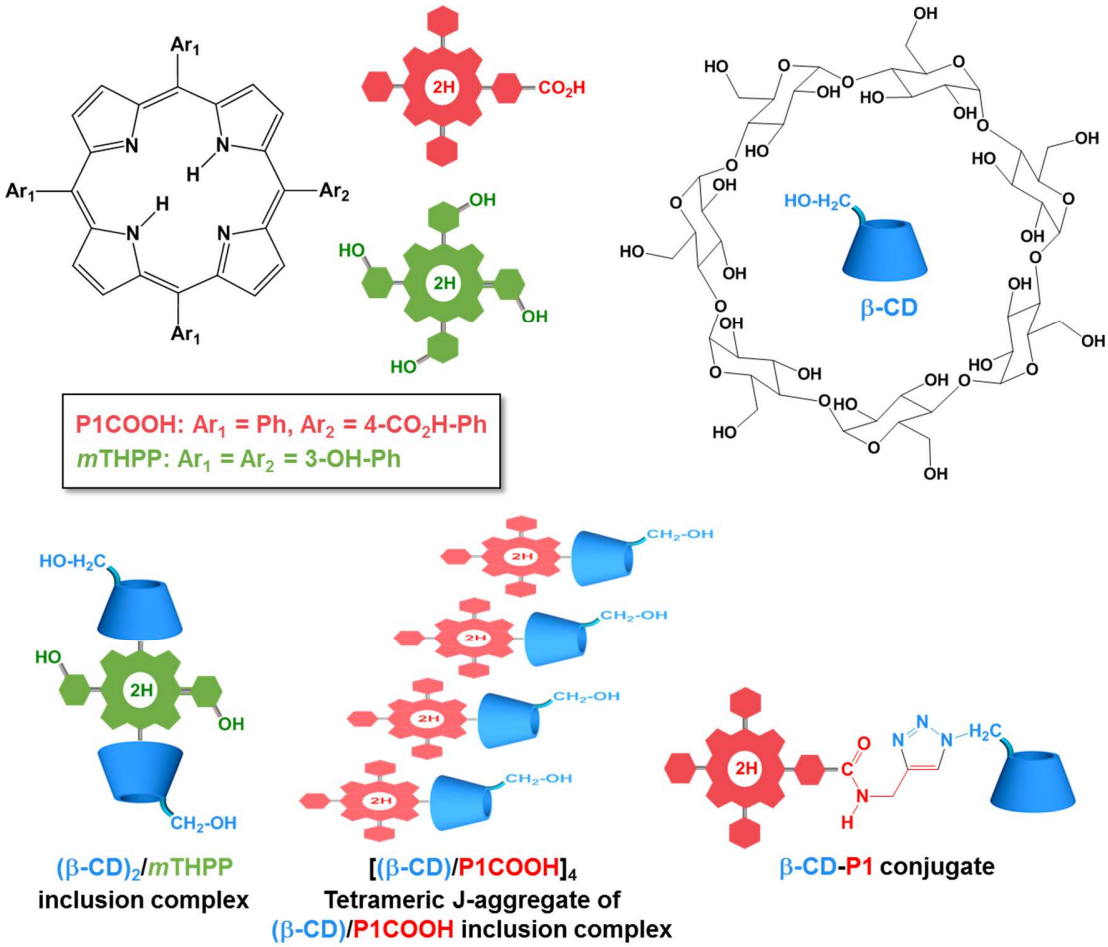

Fig. 1. Chemical structures of *m*THPP, P1COOH and β-CD, and schematic illustration of the three studied β-CD/PS systems.

2. Materials and methods

2.1. Chemicals

All chemicals were purchased as the highest purity commercially available and used without further purifications. β-CD was purchased from Sigma-Aldrich and photosensitizers (*m*THPP and P1COOH) from PorphyChem Company. All reactions involving porphyrin compounds were performed in the dark by protecting the reactors and other glassware with aluminium foil. Bioassays were evaluated on human glioblastoma U251 (Sigma-Aldrich) and U87 MG (ATCC® HTB-14 ™) cell lines.

2.2. Characterization

Reactions were monitored by thin-layer chromatography (TLC) using aluminium-backed silica gel plates (Macharey-Nagel ALUGRAM® SIL > G/UV254). TLC spots were viewed under ultraviolet light (256 nm). Porphyrin compounds purifications were performed either by flash chromatography using Geduran 60 H Silica Gel (63-200 mesh) or by reverse phase high performance liquid chromatography (HPLC) (C18 column) using methanol/water or acetonitrile/water (v/v) gradients (from 10/90 to 100/0 in 25 min, then 100/0 for 15 min). Infrared spectra were recorded with an attenuated total reflectance Fourier transform infrared (FTIR) Brucker ALPHA spectrophotometer with a wavenumber between 400 and 4000 cm^{-1}. Ultraviolet-Visible (UV-vis) absorption spectra were measured on a Shimadzu UV-3600 double-beam UV-vis spectrophotometer. Fluorescence spectra were recorded on a Fluorolog-3 spectrofluorometer FL3-222. Powder X-ray diffraction (XRD) measurements were performed using a Panalytical X'Pert Pro diffractometer equipped with a Cu tube, a Ge (111) incident beam monochromator (λ = 1, 5406 Å) and an X'Celerator detector. Data collections were recorded in the 3-70 ° scattering angle range with a pitch of 0.0167 ° for 90 min. Thermogravimetric (TG) and differential thermal (DTA) analyses were performed on a Mettler Toledo TGA/DSC1 Star System under N_2 atmosphere at a heating rate of 10 °C/min in a temperature range of 30-900 °C. ^{1}H and ^{13}C NMR spectra were recorded on a Brucker Advance 300 MHz spectrophotometer. The spectra were recorded in DMSO-d_6 at room temperature (T = 298 K) using residual DMSO peaks (δ = 2.5 ppm for ^{1}H NMR and δ = 39.5 ppm for ^{13}C NMR). Chemical shifts (δ) were reported in parts per million (ppm). Coupling constants (*J*) were given in hertz (Hz) and the multiplicity was defined as s for singlet, t for triplet, m for multiplet, br for broad, Pyr for pyrrole, Ar for aromatic or combinations thereof. Electrospray ionization high resolution mass spectrum (ESI-HRMS) was recorded on a Brucker MicrOTOF-Q HR spectrometer.

2.3. Synthesis of (β-CD)$_n$/PS inclusion complexes

2.3.1. Stoichiometry (n) and association constant (K_a) determination

Firstly, the stoichiometry (n) was determined using Job's method [20]. In brief, stock solutions of equimolar concentrations (*c* = 10 µM) of β-CD (in MeOH/milli-Q water or THF/milli-Q water, 50/50, v/v) and PS (*m*THPP in MeOH/milli-Q water or P1COOH in THF/milli-Q water, 50/50, v/v) were prepared. These solutions of β-CD and PS were mixed at various volumes to provide different samples having a constant total concentration of 10 µM, a constant total volume of 5 mL and a molar ratio of PS varying from 0 to 1. The solutions were mixed in a thermostatic mixer at 30 °C, 100 rpm for 24 h. Finally, the absorbance for all sample were measured (λ_{exc} = 415 nm) and the absorbance differences (A-A_0) were calculated and plotted against the mole fractions (r). The n value for the studied (β-CD)$_n$/PS

inclusion complex was determined with the r value at the maximum of ($A-A_0$) on the Job curve using Eq.1.

$$r = [PS]_T/([PS]_T + [\beta\text{-}CD]_T) = 1/(1+n) \quad \textbf{Eq. 1}$$

where r was the mole fraction, $[PS]_T$ and $[\beta\text{-}CD]_T$ were the total concentrations of PS and β-CD in samples, and n was the complexation order.

Secondly, the association constant (K_a) was calculated using Benesi-Hildebrand's method [21]. A 1 mL solution of PS (*m*THPP in MeOH or P1COOH in THF, c = 25 µM) was added to a 9 mL solution of β-CD at various concentrations (c = 2 mM to 20 mM). The different samples were mixed in a thermostatic mixer at 30 °C, 100 rpm for 30 min. Finally, the absorbance for all sample were measured (λ_{exc} = 415 nm) and the absorbance differences ($1/A-A_0$) were calculated and plotted against the concentrations ($[\beta\text{-}CD]_0)^n$. The K_a value for the studied $(\beta\text{-}CD)_n$/PS inclusion complex was determined with the linear relationship between $[1/(A-A_0)]$ and $([\beta\text{-}CD]_0)^n$ on the Benesi-Hildebrand curve using Eq.2.

$$1/(A-A_0) = [1/K_a \times 1/(k\times Q\times[PS]_0) \times 1/([\beta\text{-}CD_0])^n] + 1/(k\times Q\times[PS]_0) \quad \textbf{Eq. 2}$$

where $A-A_0$ was the difference between the PS's absorbance values in the presence (A) and in the absence (A_0) of β-CD, K_a was the association constant, k and Q were constants, $[PS]_0$ and $[\beta\text{-}CD]_0$ were the initial concentrations of PS and β-CD in samples, and n was the complexation order.

2.3.2. Solid $(\beta\text{-}CD)_n$/PS inclusion complexes

Solid $(\beta\text{-}CD)_n$/PS inclusion complexes were prepared using new approach by combining co-precipitation and lyophilization methods. In brief, equimolar solution of *m*THPP (or P1COOH) in MeOH (or THF) (0.2 mol, c = 20 mM) was added dropwise at room temperature to a stirred solution of the equimolar aqueous solution of β-CD (0.2 mol, c = 20 mM in milli-Q water). The reaction mixture was warmed to 60-70 °C, allowed to stir for 5 h in the dark and the organic solvent was removed under vacuum. The reaction mixture was diluted in milli-Q water and filtered through a 0.45 µm filter to remove the excess of poorly water-soluble PS. The resulted filtrates were lyophilized at -80 °C overnight in the dark and then stored at 4 °C protected from light.

The β-CD+PS physical mixtures were prepared by grinding equimolar amounts of PS and β-CD using a mortar until the obtaining of homogeneous mixtures.

2.4. Synthesis of β-CD-P1 conjugate

Porphyrin derivatives **1**-**2** were prepared in 96 % and 100 % yield, respectively, according to the protocol previously described by our team [22].

*2.4.1. Mono-6-(p-tolylsulfonyl)-β-cyclodextrin, **3***

β-CD derivative **3** was prepared using the protocol previously described by our team [23] with slight modifications. β-CD (5.0 g, 4.40 mmol, 1 equiv) was dissolved in NaOH 10 wt. % solution (70 mL) and left at 4 °C overnight. TsCl (5.0 g, 26.2 mmol, 6 equiv) was added in three equal portions to the β-CD solution at 0 °C under vigorous stirring. 5 h later, the resulted mixture was purified by filtration the resulted mixture was purified by filtration on Celite® through a fritted-glass funnel with 3 µm frit porosity. The filtrate was precipitated at 0-5 °C by adjusting the pH to 1-2 with concentrated HCl solution and stored overnight at 4 °C. The precipitate was then filtered under vacuum, recrystallized three times in hot ultra-pure water and dried overnight at 50 °C to provide **3** as a white powder. The characterization of **3** is in agreement with those previously described in the literature [24]. ^{1}H NMR (300 MHz, DMSO-d_6) δ = 2.0 (s, 3H, CH_3 tosyl), 2.93-3.42 (m, 14 H, H4 and H2), 3.43-3.83 (m, 28H, H3, H5 and H6), 4,22-4.42 (m, 6H, OH6), 4,75 (br s, 1H, H1), 4.83 (br s, 6H, H1), 5.45-5.95 (br s, 14H, OH2 and OH3), 7.43 (d, 2H, *J* = 8.1 Hz, H9), 7,74 (d, 2H, *J* = 8.1 Hz, H8).

2.4.2. β-CD-P1 conjugate

β-CD derivative **4** was prepared in 96 % yield according to the protocol previously described in the literature [24]. $CuSO_4.5H_2O$ (0.1 equiv) and sodium ascorbate (0.5 equiv) were successively added to an equimolar mixture of **2** and **4** (0.1 mmol, 1 equiv) in H_2O/THF (4/5, v/v, 5 mL). The mixture was refluxed under vigorous stirring at 40 °C for 5 h in the dark. The reaction mixture was then cooled to room temperature and washed with milli-Q water (3 x 20 mL), dried over $MgSO_4$, and concentrated under reduced pressure. The crude product was purified by preparative HPLC to finally give a green powder of the β-CD-P1 conjugate. ^{1}H NMR (300 MHz, DMSO-d_6) δ = -2.92 (s, 2H, 2 NH pyr), 3.16-3.85 (m, overlap with HDO, 28H, 7 H2, 7 H3, 7 H4, 7 H5 and 14 H6), 4.05-4.62 (m, 7 OH6), 4.70 (br s, 2H, CH_2-NH), 4.83 (br s, 6H, H1), 5.10 (br s, 1H, H1), 5.74 (br s, 14H, 7 OH2 and 7 OH3), 7.72-7.92 (m, 9H, H Ar), 8.06 (s, 1H, CH triazole), 8.15-8.30 (m, 8H, H Ar), 8.32 (s, 2H, H Ar), 8.84 (s, 8H, H_β pyr), 9.34 (t, 1H, J = 5.7 Hz, NH amide). ^{13}C NMR (75 MHz, DMSO-d_6) δ = 35.0 (CH_2-NH), 59.9 (C_6), 72.0 (C2, C3 or C5), 72, 4 (C2, C3 or C5), 73.0 (C2, C3 or C5), 81.5 (C4), 101.9 (C1), 119.0 (C Ar), 120.1 (C Ar), 125.9 (CH triazole), 126.0 (CH Ar), 128.1 (CH Ar), 132.3 (CH_β), 134.2 (CH Ar), 141.1 (C Ar), 144.1 (C

Ar), 144.6 (C triazole), 157.8 (C Ar), 166.3 (C=O). HRMS calculated for $C_{90}H_{102}N_8O_{35}$ $[M+2H]^+/2$ m/z 928.8243; found 928.8271 (see Supporting Information, Figs. S1-S5).

2.5. *Disaggregation study in aqueous medium*

A fixed concentration of PS (*m*THPP or P1COOH, c = 2 µM) was used in the disaggregation study and prepared by dissolution in a minimum of organic solvent (MeOH for *m*THPP and THF for P1COOH) followed by dilution in milli-Q water. A 0.5 mL solution of PS was added to a 4.5 mL aqueous solution of β-CD in milli-Q water at various concentrations. The resulted PS+β-CD solutions were warmed to 40 °C and stirred for 30 min. The UV-vis absorption and fluorescence emission spectra were then recorded and compared.

2.6. *Binding type effect on PSs disaggregation in aqueous medium*

The binding type effect of β-CD on the disaggregation in aqueous medium of *m*THPP and P1COOH in the different β-CD/PS systems was studied by comparing their UV-vis, fluorescence and $^1O_2$ luminescence spectra to those of free PSs in the same conditions. Briefly, aqueous solutions were prepared by direct dissolution of each product in D_2O ((β-CD)$_2$/*m*THPP and [(β-CD)/P1COOH]$_4$) or by dissolution in a minimum of DMSO followed by dilution in D_2O (β-CD-P1, *m*THPP and P1COOH). The UV-vis absorption and fluorescence emission spectra were recorded at 200-800 nm and 600-800 nm wavelength ranges, respectively. Fluorescence (ϕ_f) and singlet oxygen (ϕ_Δ) quantum yields were determined using tetraphenyl porphyrin (TPP) solution in toluene as fluorescence standard (ϕ_f = 0.11) [25] and Rose Bengal solution in D_2O as $^1O_2$ reference (ϕ_Δ = 0.76) [26]. The absorbance value at the excitation wavelength of the reference and the sample solutions were set around 0.2.

2.7. *In vitro PDT activity*

2.7.1. *Cell culture conditions*

Human glioblastoma U251 or U87 cells were cultured in DMEM (Dulbecco's Modified Eagle Medium) supplemented with sodium pyruvate (1.5 mM) and vitamins MEM AA, MEM NE AA, L-Ser (14 µg/mL), L-asp (25 µg/mL), L-Glu (2.5 mM), penicillin (100 U/mL), streptomycin (100 µg/mL) and 20 % fetal calf serum (FCS) under standard cell culture conditions at 37 °C in a humidified atmosphere (80 %) containing 5 % CO_2.

197 *2.7.2. In vitro photodynamic activity*

198 The dark cytotoxicity and phototoxicity of tested compounds (β-CD/PS systems, free PSs and β-CD) were
199 performed on human glioblastoma U87 and U251 cells after incubation in the dark (dark cytotoxicity) or
200 after exposure to light (phototoxicity). Cell viability was determined by measuring the activity of live cell
201 mitochondrial dehydrogenases (MTT assay) as previously described [27]. Briefly, cancer cells were
202 seeded at 2 x 10^4 cells/cm^2. The stock solutions of the tested compounds were prepared in HBSS (Hank's
203 Balanced Salt Solution) (2 mg/mL) and then diluted to the required concentrations in the DMEM culture
204 medium. Free *m*THPP, free P1COOH and β-CD-P1 conjugate were first dissolved in a minimum of
205 DMSO and the resulted solutions were diluted in the DMEM culture medium (it is important to note that
206 the concentration of the final DMSO not exceeded 0.25 %). After 48 h, the initial culture medium was
207 removed and the cancer cells were treated with each compound separately at a final PS concentration of 1,
208 2 and 3 µM for U87 cells, and treated only with β-CD-P1 conjugate at a final PS concentration of 1, 2, 3,
209 5, 10 and 20 µM for U251 cells. The cells were incubated in the dark for another 24 h. The cancer cells
210 were then washed three times with HBSS to remove the non-internalized tested compounds and a new
211 culture medium was added. In order to study the cytotoxic effect of the tested compounds, cancer cells
212 were kept in the dark. The photoinduced toxicity of these tested compounds was estimated by exposing
213 the cells to light (4.54 mW/cm^2, fluence 10 J/cm^2) using a 652 nm diode laser system for 36 min. After
214 treatment, the cancer cells were incubated for an additional 24 h under standard culture conditions. The
215 viability of the cancer cells was evaluated using the MTT assay: 0.4 mg/mL of MTT (3-(4,5-
216 dimethylthiazol-2-yl)-2,5-diphenyltetrazolium bromide) was added to each well and the plates were then
217 incubated for 3 h at 37 °C. The old media was removed, and DMSO added to lyse the cells and dissolve
218 the formazan crystals that appeared in living cells. The absorbance of formazan was measured at
219 wavelength of 540/630 nm (Multiscan Ascent microplate reader). Cell viability was expressed in terms of
220 percentage of living cells *vs.* values obtained from untreated cells.

221 *2.7.3. Statistical analysis*

222 All *in vitro* experiments were realized in triplicate and the results were given as mean ± standard
223 deviation (SD). Differences among groups were evaluated using variance analysis (Anova) followed by
224 Bonferroni test (GraphPad Prism 6.0 software). A value of $p < 0.05$ was considered as statistically
225 significant. * *Vs.* control cells, # *vs.* same compound at smaller concentration used.

226 **3. Results and discussion**

3.1. *Stoichiometry (n) and association constant (K_a) determination*

Prior to starting the synthesis of solid (β-CD)n/PS inclusion complexes of *m*THPP or P1COOH as guest and β-CD as host, it is critical to determine both the stoichiometry (n) and the association constant (K_a) in the host-guest interaction. The classical methods employed to access the n and Ka values are Job's (continuous variation method) [20] and Benesi-Hildebrand's [21] methods using Eq.1 and Eq.2, respectively (see Section 2.3.1.).

For the β-CD/*m*THPP system, the Job's continuous variation plot (Fig. 2A) reveals a maximum absorbance at the r value of 0.33 mole (at λ = 415 nm), corresponding to the n value of 2 from Eq. 1, indicating the formation of the $(\beta\text{-CD})_2$/*m*THPP inclusion complex. The Benesi-Hildebrand plot (Fig. 2B) of measured absorbance $[1/(A-A_0)]$ at 415 nm *vs.* $([\beta\text{-CD}]_0)^2$ (n = 2) shows a linear relationship with a correlation (R^2) of 0.9993. By considering the 2:1 complex stoichiometry between β-CD and *m*THPP, an association constant K_a of 1.2045 10^4 M^{-2} is determined from Eq. 2 and linear relationship between $[1/(A-A_0)]$ and $([\beta\text{-CD}]_0)^2$.

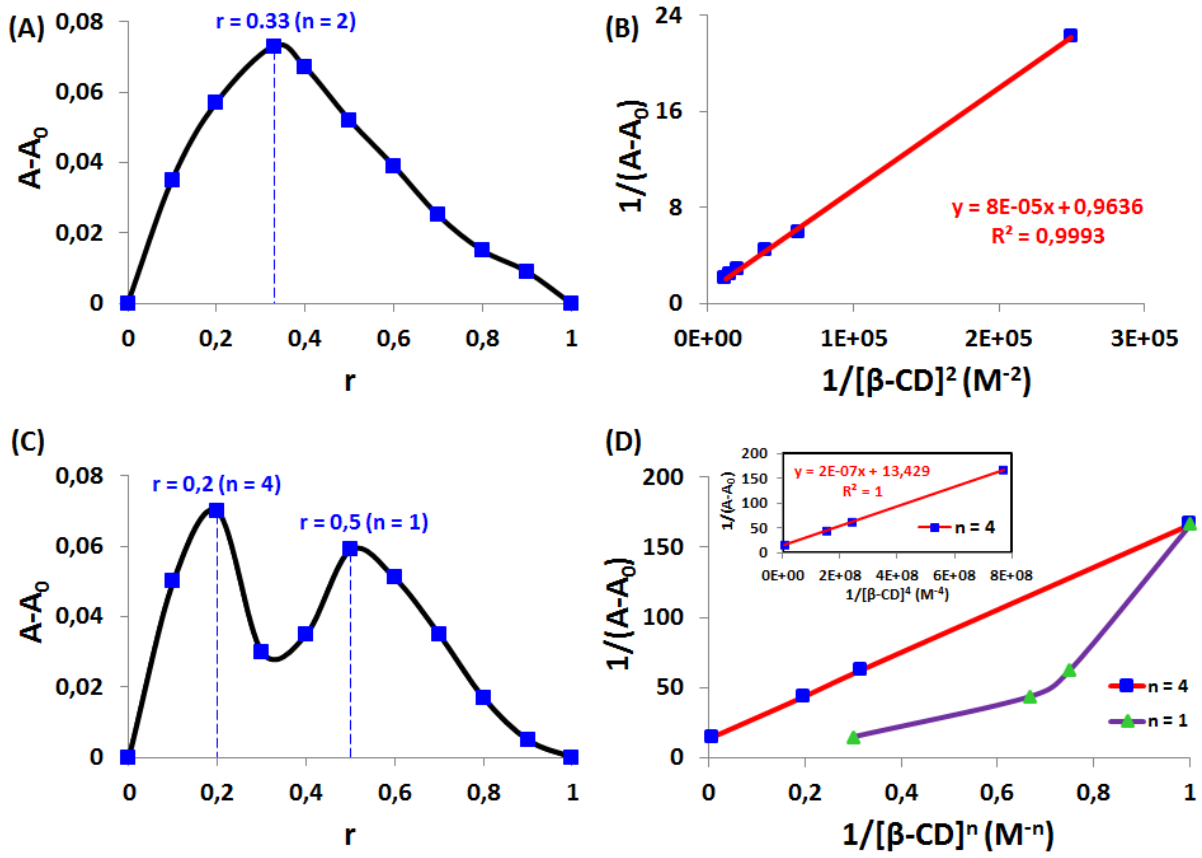

Fig. 2. (A) Job's and (B) Benesi-Hildebrand plots for complexation of *m*THPP with β-CD determined by UV-vis absorption at 415 nm. (C) Job's and (D) Benesi-Hildebrand plots for complexation of P1COOH with β-CD determined by UV-vis absorption at 415 nm.

For the β-CD/P1COOH system, the Job's continuous variation plot (Fig. 2C) shows some interesting behaviour exhibiting two maxima at 1:1 and 4:1 stoichiometric ratios for the $(\beta\text{-CD})_n$/P1COOH inclusion complex. The Benesi-Hildebrand plot (Fig. 2D) reveals a linear relationship with a correlation (R^2) of 1 (K_a = 3.723 10^4 M^{-4}) for the 4:1 ratio only, which means that the inclusion complex involving 4 β-CDs is the most stable. However, there is one major remaining question: Does the most stable 4:1 inclusion complex from Job's plot is due to coordination of 4 β-CDs to the non-aggregated (*i.e.* monomeric species, 4:1 inclusion complex) as well as aggregated P1COOH (*i.e.* tetrameric species, self-aggregation of four 1:1 inclusion complexes). The answer to this question is given by the spectroscopic studies in aqueous medium (see Sections 3.4. and 3.5.). In general, the inclusion complex with cyclodextrin does not affect the UV-vis spectrum of small molecules but, in our case, the UV-vis spectrum of the inclusion complex reveals a remarkable red shift of the Soret band indicating that a phenomenon of J-aggregation occurs in this inclusion complex [28]. The aggregation phenomenon is also evidenced by the fluorescence emission and $^1O_2$ luminescence quenching which is due to the self-aggregation of PSs in aqueous medium through π–π stacking due to their hydrophobic and rigid planar structures [29-31]. All these data highlight the presence of an inclusion complex with the 4 β-CDs in an aggregate form (*i.e.* tetrameric species, self-aggregation of four 1:1 inclusion complexes, Fig. 1). It should be noted that the obtaining of a Job's plot with two peaks is possible but quite rare. For example, P. Tau et al. in 2003 synthetized an inclusion complex between β-CD and a tetrasubstituted zinc phthalocyanine (ZnPc) and obtained also a Job's plot with 2 peaks [32]. The authors observed two maxima at inclusion ratios of about 2:1 and 4:1 (β-CD:ZnPc), and came to the same conclusion as we did above, that the 2:1 corresponded to the coordination of 2 β-CDs to the non-aggregated complex (*i.e.* monomeric species, 2:1 inclusion complex) and 4:1 to the coordination of 4 β-CDs to the aggregated complex (*i.e.* dimeric species, self-aggregation of two 2:1 inclusion complexes).

3.2. Synthesis and characterization of solid $(\beta\text{-CD})_n$/PS inclusion complexes

With evidence now conclusive that inclusion complexes of *m*THPP or P1COOH as guest and β-CD as host can be formed, preparation of solid $(\beta\text{-CD})_2$/*m*THPP and $[(\beta\text{-CD})/\text{P1COOH}]_4$ inclusion complexes is tackled for the first time using a new co-precipitation@lyophilization combined method. Solid inclusion

complexes formation is confirmed by studying the host-guest interactions with different experiments including ^{1}H NMR, FTIR, TG and DTA, and XRD.

^{1}H NMR spectroscopy is one of the powerful experimental techniques for the investigation of the successful preparation of inclusion complexes [33]. The formation of a $(\beta\text{-CD})_n$/PS inclusion complex is based on intermolecular interactions between PS and β-CD, resulting in changes in chemical shifts of β-CD. It is generally accepted, for β-CD, that the chemical shift values of H3 and H5 protons (located inside the cavity) are more variable than H2, H4 and H6 protons when the inclusion complex is formed [34,35]. ^{1}H chemical shifts (δ) values for H1-H6 protons in β-CD and solid $(\beta\text{-CD})_2$/*m*THPP and $[(\beta\text{-CD})/\text{P1COOH}]_4$ inclusion complexes are given in Table 1 and confirm the successful preparation of both inclusion complexes.

Table 1. ^{1}H chemical shifts (ppm) values for H1-H6 protons in β-CD and solid $(\beta\text{-CD})_2$/*m*THPP and $[(\beta\text{-CD})/\text{P1COOH}]_4$ inclusion complexes (300 MHz, DMSO-d_6, 298K).

Compound	H1	H2	H3	H4	H5	H6
β-CD	4.829	3.301	3.659	3.375	3.577	3.630
$(\beta\text{-CD})_2$/*m*THPP	4.831	3.304	3.678	3.377	3.599	3.637
$\Delta\delta^a$	+0.002	+0.003	+0.019	+0.002	+0.022	+0.007
$[(\beta\text{-CD})/\text{P1COOH}]_4$	4.830	3.301	3.675	3.378	3.595	3.632
$\Delta\delta^b$	+0.001	+0.000	+0.016	+0.003	+0.018	+0.002

[a]: $\Delta\delta = \delta((\beta\text{-CD})_2/m\text{THPP}) - \delta(\beta\text{-CD})$; [b]: $\Delta\delta = \delta([(\beta\text{-CD})/\text{P1COOH}]_4) - \delta(\beta\text{-CD})$.

FTIR is widely used to confirm the inclusion complex formation because, in general, the included part of the guest entity is shifted, disappears or its intensity is altered [36,37]. FTIR spectra of β-CD, PS, physical mixture β-CD+PS and $(\beta\text{-CD})_n$/PS inclusion complex for *m*THPP and P1COOH are shown in Fig. 3. The FTIR spectrum of β-CD consists of the broad O-H stretching band centered at 3278 cm^{-1}, the symmetric and asymmetric C-H stretching bands at 2979 and 2900 cm^{-1}, the H-O-H deformation bands at 1643 cm^{-1} due to water molecules present in β-CD, the C-O-C vibrational band at 1151 cm^{-1}, the broad C-H and C-O stretching bands around 1026 cm^{-1}. Concerning the PSs, the FTIR spectra reveal various characteristic bands relating to major functional groups contained in *m*THPP and P1COOH. Among these functional groups, we would cite the N-H stretching bands at 3250 cm^{-1}, the C=C stretching bands of the benzene ring at 1583 and 1433 cm^{-1}, the C-O stretching band at 1234 cm^{-1} for *m*THPP, and the N-H stretching bands at 3315 cm^{-1}, the C=O stretching bands of the free acid at 1682 cm^{-1}, the C-C and C-H bending bands of the free base pyrrole around 961 cm^{-1} for P1COOH. In one hand, FTIR spectra of β-CD+PS

physical mixtures (β-CD+*m*THPP and β-CD+P1COOH) merely consist of the sum of the PS (*m*THPP or P1COOH) and β-CD spectra without apparent changes. On the other hand, the FTIR spectra of $(\beta\text{-CD})_n$/PS inclusion complexes ($(\beta\text{-CD})_2$/*m*THPP and $[(\beta\text{-CD})/\text{P1COOH}]_4$) are different from those of the β-CD+PS physical mixtures and reveal important changes in several regions *(i.e.* decreased intensity, disappearance or shifting of some bands related to β-CD and PS). These changes are due to the microenvironment modifications encountered in the establishment of hydrogen bonds and van der Waals interactions between β-CD and PSs during the formation of inclusion complexes [31]. As regards the change in the C=C stretching bands of the benzene ring of *m*THPP in the $(\beta\text{-CD})_2$/*m*THPP inclusion complex, the peak at 1433 cm^{-1} is shifted towards 1414 cm^{-1} and the intensity of the peak at 1583 cm^{-1} become very low until it completely disappeared. These two observations suggest that one or more of the aromatic rings of *m*THPP is inside the β-CD cavity. We may also mention the change in the C-C and C-H bending bands of the free base pyrrole of P1COOH in the $[(\beta\text{-CD})/\text{P1COOH}]_4$) inclusion complex, the peak at 961 cm^{-1} is shifted towards 996 cm^{-1} indicating interactions between β-CD and the C-C and C-H groups of the free base pyrrole rings of P1COOH. To conclude we may add that the broad O-H stretching band of β-CD centered at 3278 cm^{-1} is shifted at 3310 cm^{-1} in both inclusion complexes signaling the establishment of hydrogen bonds between β-CD and PSs. The FTIR spectroscopy study confirms the formation of $(\beta\text{-CD})_2$/*m*THPP and $[(\beta\text{-CD})/\text{P1COOH}]_4$ inclusion complexes and shows that grinding method is not appropriate to form the both inclusion complexes.

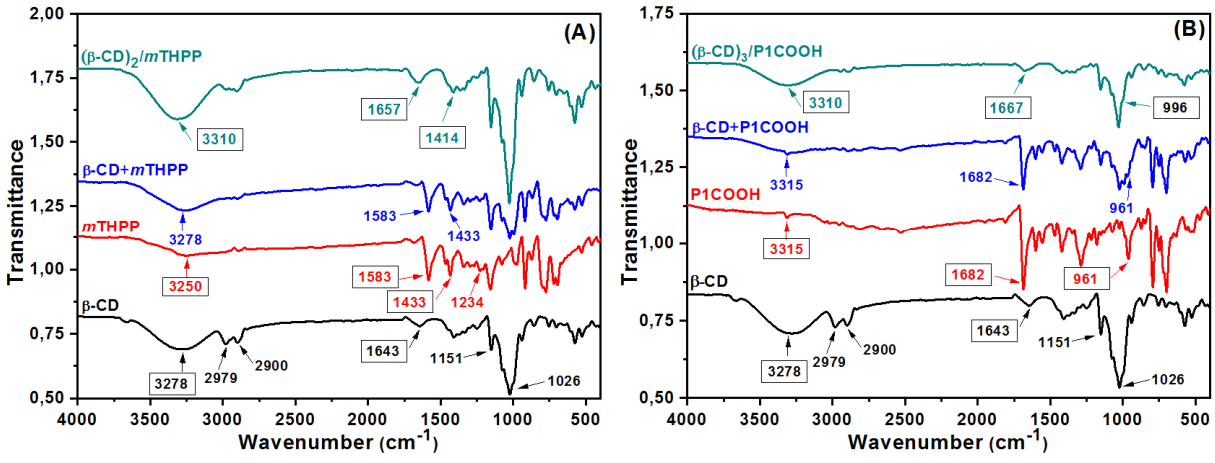

Fig. 3. FTIR spectra of β-CD, PS, β-CD+PS physical mixture and $(\beta\text{-CD})_n$/PS inclusion complex for (A) *m*THPP and (B) P1COOH.

Another evidence of solid inclusion complexes formation is provided by thermal analyses. Among the various thermal analyses, mention may be made of complementary analyses TG and DTA. TG analysis

allows studying the change in the weight of the solid sample as a function of time. DTA may be considered as complementary method to TG analysis of studying inclusion complexes. TG and DTA curves (top and bottom figure, respectively) of β-CD, PS, physical mixture β-CD+PS and $(\beta\text{-CD})_n$/PS inclusion complex for *m*THPP and P1COOH are shown in Fig. 4. TG and DTA curves of β-CD display two zones where there is a weight loss of β-CD (Zones 1 and 2) that are associated with two endothermic processes. The first zone (Zone 1) at around 92 °C with a 10 % weight loss can be attributed to a dehydration process of β-CD while the second zone (Zone 2) around 324 °C with a 80 % weight loss can be assigned to the fusion and decomposition of β-CD [37]. As regards the PSs (*m*THPP and P1COOH), TG and DTA thermograms exhibit a continuous decomposition process beginning at around 150-200 °C with a 4-5 % weight loss which could be assigned to a dehydration process of PSs, followed by a major stage around 400-600 °C. This major stage can be divided in two small sub-regions (Zones 3 and 4) which can be related to the decomposition process of the porphyrin rings (*i.e.* loss of chains of the porphyrin rings and decomposition of the porphyrin macrocycles). The two small sub-regions are located at 396 °C (8 % weight loss, Zone 3) and 409 °C (22 % weight loss, Zone 4) for *m*THPP, and at 438 °C (13 % weight loss, Zone 3) and 510 °C (16 % weight loss, Zone 4) for P1COOH. For the TG and DTA curves of the physical mixtures β-CD+*m*THPP and β-CD+P1COOH, the thermal behaviours are the sum of the thermal behaviours of free precursors β-CD and PS (*m*THPP or P1COOH), meaning that no interactions are established between β-CD and PSs. However, in the TG and DTA curves of the $(\beta\text{-CD})_2$/*m*THPP and $[(\beta\text{-CD})/\text{P1COOH}]_4$ inclusion complexes, the characteristic thermal curves of PSs between 400 and 600 °C disappear, which in turn suggests the establishment of interactions between β-CD and PSs and thus the solid inclusion complexes formation.

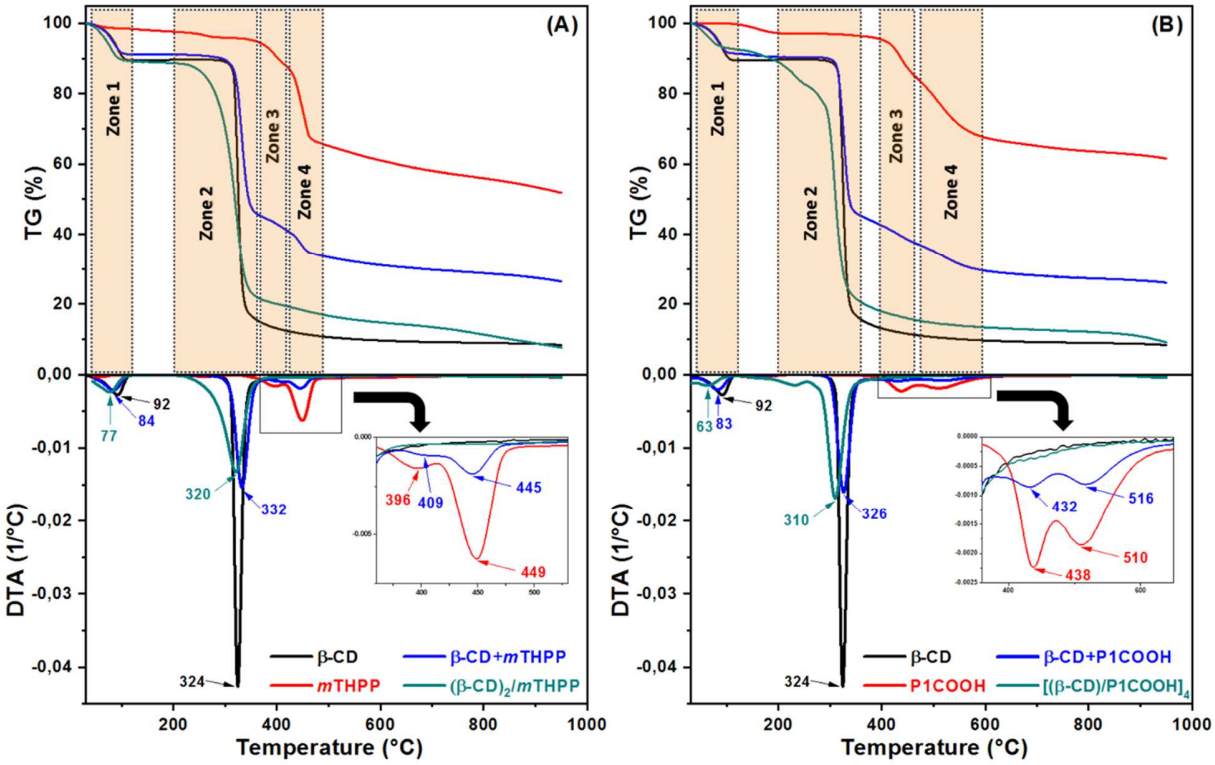

Fig. 4. TG (top) and DTA (bottom) curves for β-CD, PS, β-CD+PS physical mixture and $(\beta\text{-CD})_n$/PS inclusion complex for (A) *m*THPP and (B) P1COOH.

The latest striking evidence of the solid $(\beta\text{-CD})_2$/*m*THPP and $[(\beta\text{-CD})/\text{P1COOH}]_4$ inclusion complexes formation comes from XRD analysis. The powder XRD patterns in the 2θ range of 5°-30° of β-CD, PS, β-CD+PS physical mixture and $(\beta\text{-CD})_n$/PS inclusion complex for *m*THPP and P1COOH are shown in Fig. 5. The XRD diffractogram of β-CD (like P1COOH) reveals a series of sharp and intense crystalline peaks [38,39] while *m*THPP is amorphous with broad diffraction peaks distributed in a wide 2θ range. Compared with the XRD patterns of the physical mixtures containing all peaks of β-CD and PSs with a slight change of intensity and position, the sharp crystalline peaks of β-CD disappear in the XRD patterns of the solid inclusion complexes, confirming the spatial entrapment of PSs inside de cavity of β-CD and thus the inclusion complexes formation.

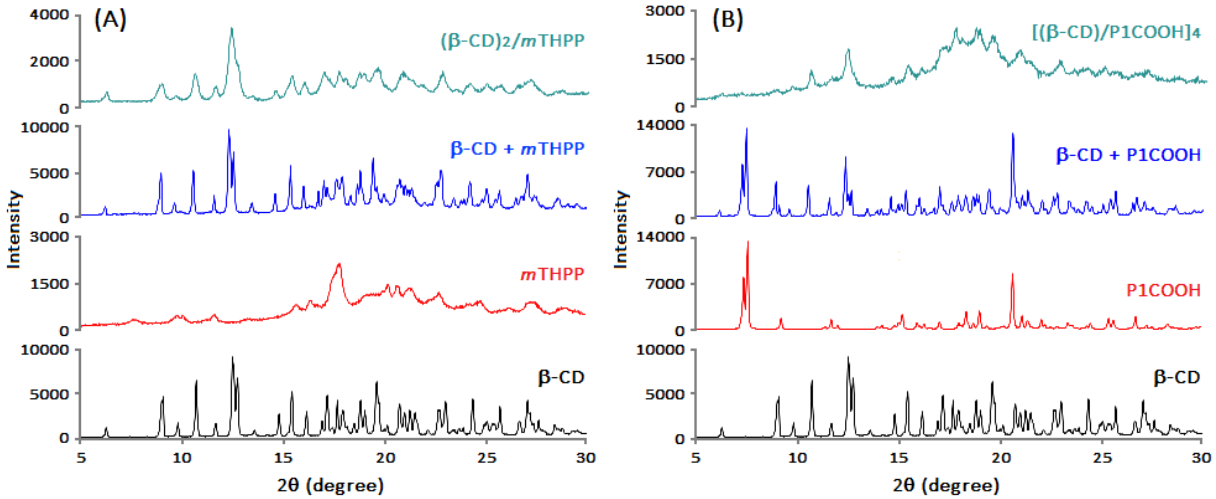

Fig. 5. Powder XRD patterns of β-CD, PS, β-CD+PS physical mixture and $(β\text{-CD})_n$/PS inclusion complex for (A) *m*THPP and (B) P1COOH.

3.3. Synthesis of β-CD)-PS conjugate

In parallel to the preparation of the solid $(β\text{-CD})_n$/PS inclusion complexes with non-covalent bonding between β-CD and PSs, the synthesis of covalent conjugate β-CD-P1 was also undertaken by combining P1COOH with β-CD *via* a triazole covalent link. Only P1COOH as PS was used with the aim of providing exclusively the mono-functionalization of the PS with β-CD. The triazole covalent link was obtained by CuAAC click chemistry. To achieve this goal, propargyl-modified ZnP1COOH **2** and azide-modified β-CD **4** were prepared (Fig. 6).

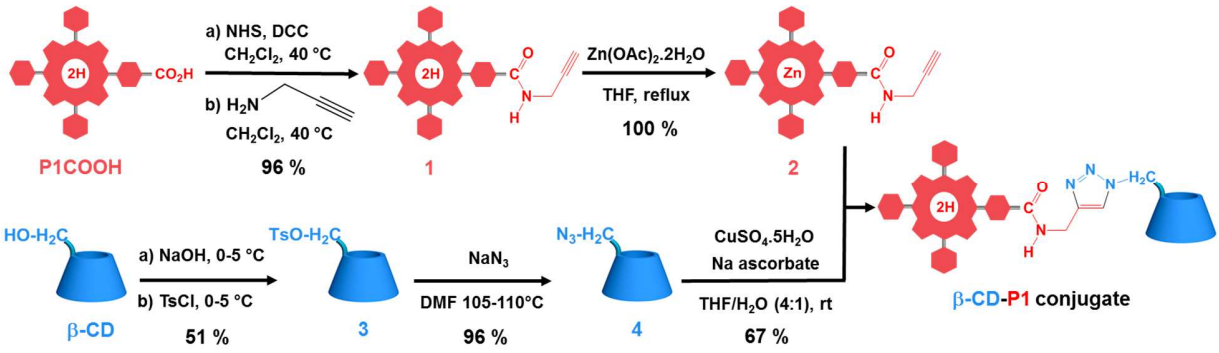

Fig. 6. Synthetic route for β-CD-P1 conjugate.

Propargyl-modified ZnP1COOH **2** was prepared in two steps with 96 % overall yield according to the protocol previously described by our team (Fig. 6) [22]. First, the carboxylic function of P1COOH was

activated *in situ* as NHS ester using dicyclohexylcarbodiimide (DCC) and *N*-hydroxysuccinimide (NHS), then coupled with propargylamine to afford the propargyl-modified P1COOH **1** in 96 % yield. Secondly, the porphyrin ring of **1** was metalated with $Zn(OAc)_2$ to provide the desired propargyl-modified ZnP1COOH **2** in quantitative yield. The metalation step was essential to avoid copper metalation of the porphyrin ring during the subsequent CuAAC reaction.

Azide-modified β-CD **4** was prepared in two-step procedure in 49 % overall yield (Fig. 6). First, the secondary hydroxyl groups of β-CD were tosylated using tosyl chloride to provide β-CD-OTs **3** in 51 % yield according to a previous protocol described by our team [23] with slight modifications. Second, tosyl groups of β-CD-OTs **3** were subjected to a nucleophilic substitution with sodium azide to provide azide-modified β-CD **4** in 96 % yield according to a previous protocol described in the literature [24].

Finally, the synthesis of the conjugate β-CD-P1 was obtained using CuAAC click chemistry between **2** and **4** *via* triazole covalent link formation in 67 % yield (Fig. 6). It is noted that the demetalation of the porphyrin ring occurred during the purification step.

3.4. Disaggregation study in aqueous medium

The disaggregation effect of β-CD on PS (*m*THPP or P1COOH) in aqueous medium is investigated using a fixed PS concentration of 2 µM and a varied β-CD concentration from 0 to 50 mM. The UV-vis absorption and fluorescence emission spectra of PS with different concentrations of β-CD are shown in Fig. 7. UV-vis spectrum of *m*THPP in milli-Q water displays the presence of very broad Soret band which is due to the combination of aggregates and monomers of *m*THPP without the possibility to assign a specific wavelength for each species (Fig. 7A). Addition of β-CD (from 0 to 7.2 mM) is found to make the Soret band more narrow leading us to deduce by deconvolution that the very broad Soret band consists of two superimposed bands located at 418 nm and 442 nm. It is generally accepted that a red-shift in the UV-vis absorption spectra relatively to that of the monomer is proof of J-aggregate and also aggregation leads to the fluorescence quenching [40]. As shown in Fig. 7A, the absorbance intensity of the peak at 418 nm and the fluorescence intensity increase significantly with the increasing concentration of β-CD, which allows assigning the peaks at 418 nm and 442 nm to *m*THPP monomers and J-aggregates, respectively. Furthermore, it is worth noting that generally, the formation of an inclusion complex with cyclodextrins does not affect the UV-vis spectrum of small molecules [41]. Based on this information, we can also assign the peak at 418 nm to the monomeric inclusion complex between *m*THPP and β-CD. All these results highlight the β-CD's ability to reduce the formation of *m*THPP aggregates through the formation of monomeric inclusion complex. The UV-vis spectrum of P1COOH in milli-Q water shows

also a similar broad Soret band to *m*THPP (Fig. 7B) and the same results can be expected. Surprisingly, a noticeable decrease of the P1COOH monomers peak at around 420 nm is observed with the addition of β-CD (from 0 to 50 mM), accompanied by the appearance of an isosbestic point in the absorption spectra at 443 nm and an increasing absorption at 472 ppm (Fig. 7B). Furthermore, the fluorescence intensity decreases notably with the increasing concentration of β-CD indicating that a phenomenon of aggregation still occurs. The presence of the isosbestic point and the red shifted peak at 472 nm confirm the formation of the inclusion complex and seem to indicate the establishment of an equilibrium between monomeric inclusion complex (420 nm) and unknown J-aggregates (472 nm). Based on the results obtained from Job's and Benesi-Hildebrand plots (see Section 3.1.), the peak at 472 nm can be assigned to J-tetramer aggregates of the 1:1 inclusion complex.

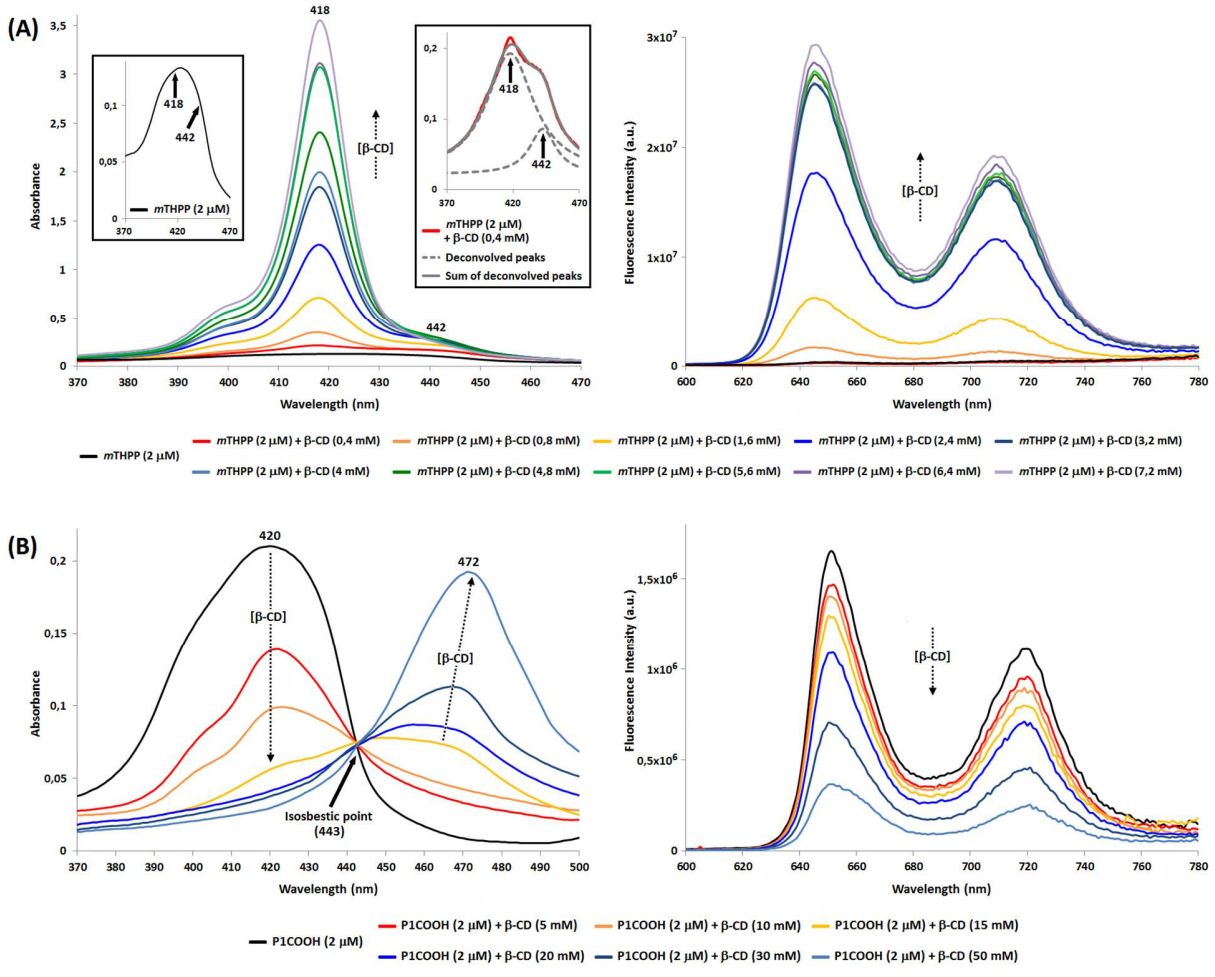

Fig. 7. UV-vis and fluorescence spectra of (A) *m*THPP (2 µM) and (B) P1COOH (2 µM) containing various concentration of β-CD in milli-Q water.

3.5. *Binding type effect on PSs disaggregation in aqueous medium*

The binding type effect of β-CD on the disaggregation of PSs (*m*THPP or P1COOH) in aqueous medium is investigated by comparing the photophysical properties of the free PSs and β-CD/PS systems in D_2O. The UV-vis absorption, fluorescence emission and $^1O_2$ luminescence spectra of the three β-CD/PS systems in D_2O are given in Fig. 8. The UV-vis spectra of the free *m*THPP and P1COOH in DMSO are characterized by a narrow Soret band (monomeric species, disaggregated state) at 421 nm and 419 nm, respectively, and four Q bands between 510 and 650 nm for each one (insert in the top right of the Fig. 8A). Coherence-consistent changes are observed on the UV-vis spectra of the two PSs when D_2O is used as solvent. The appearance of very broad Soret bands in UV-vis spectra of the free PSs in D_2O (Fig. 8A, pink and green curves), accompanied by their fluorescence emission and $^1O_2$ luminescence quenching (Figs. 8B and 8C, pink and green curves), reveal the propensity of these PSs to self-aggregate in D_2O [42]. As already observed in the disaggregation study with *m*THPP (see Section 3.4.), the UV-vis spectrum of $(\beta\text{-CD})_2$/*m*THPP inclusion complex shows an increase in absorbance intensity and sharpening of the Soret band at 418 nm compared to free *m*THPP (Fig. 8A, pink and black curves), indicating a significantly lower degree of aggregation and thus the formation of the monomeric inclusion complex in D_2O. The formation of the $(\beta\text{-CD})_2$/*m*THPP inclusion complex in monomeric form in D_2O is also evidenced by an increase of the fluorescence emission and $^1O_2$ luminescence (Figs. 8B and 8C, black curves) with fluorescence and $^1O_2$ quantum yields of 1 % and 16 %, respectively. Compared to P1COOH alone, the UV-vis spectrum of $[(\beta\text{-CD})/\text{P1COOH}]_4$ inclusion complex in D_2O shows a slight broadening and remarkable red shift of the Soret band from 420 nm to 472 ppm (Fig. 8A, green and blue curves), as already observed in the disaggregation study with P1COOH (see Section 3.4.), revealing the existence of a phenomenon of aggregation and the formation of J-tetramer aggregates of the 1:1 inclusion complex. The high J-type self-aggregation of $[(\beta\text{-CD})/\text{P1COOH}]_4$ inclusion complex in D_2O is also supported by fluorescence emission and $^1O_2$ luminescence quenching (Figs. 8B and 8C, blue curves). Finally, in contrast to a non-covalent link between P1COOH and β-CD in $[(\beta\text{-CD})/\text{P1COOH}]_4$ inclusion complex, the use of a covalent bond in β-CD-P1 conjugate shows similar observations to those made for the $(\beta\text{-CD})_2$/*m*THPP inclusion complex in D_2O, *i.e.* increased intensity and sharpening of the Soret band at around 420 nm compared to P1COOH (Fig. 8A, green and orange curves) with an increase of the fluorescence emission and $^1O_2$ luminescence yielding fluorescence and $^1O_2$ quantum yields of 2 % and 16 %, respectively (Figs. 8B and 8C, orange curves). These observations demonstrate that the use of a covalent link between P1COOH and β-CD allows the formation of the monomeric species (non-aggregated β-CD-P1 conjugate) in D_2O.

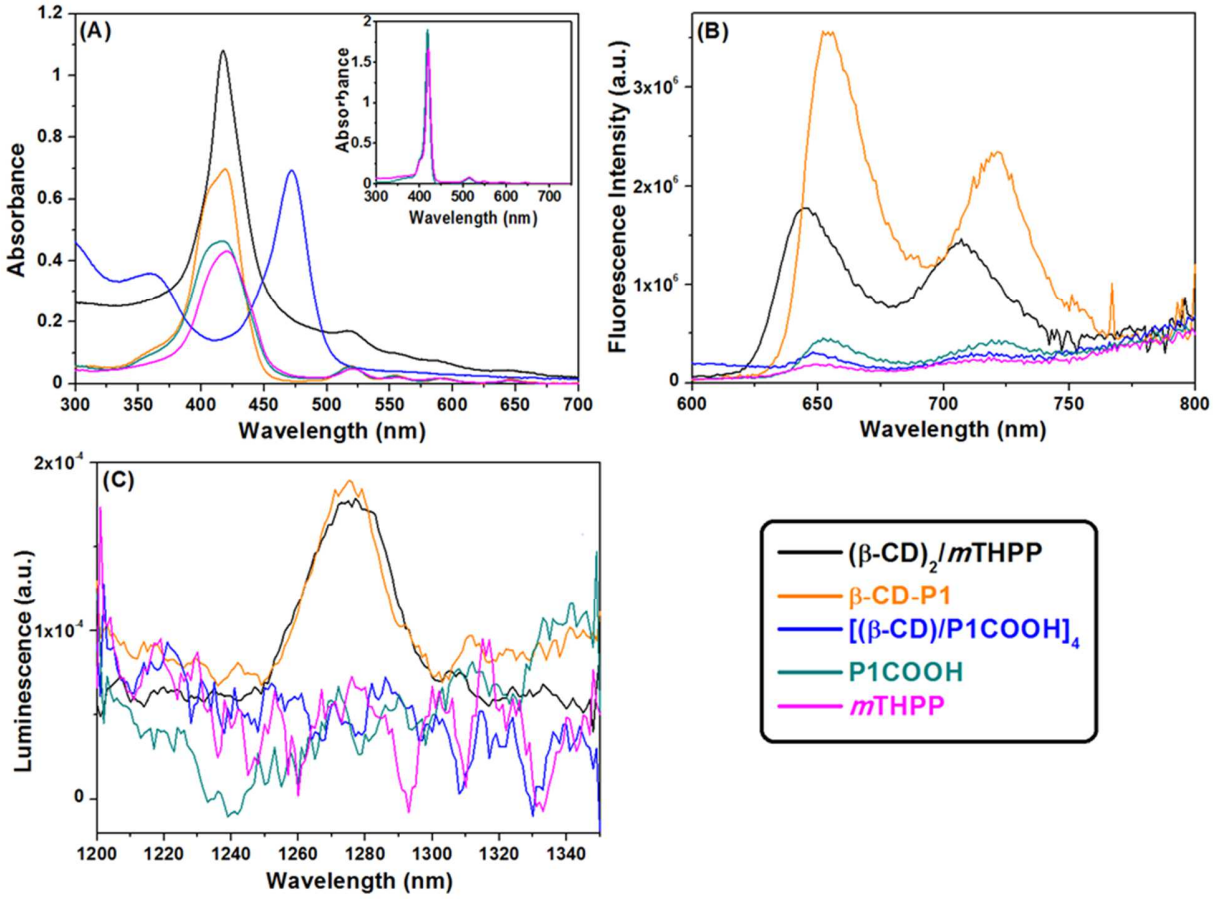

Fig. 8. Photophysical properties of *m*THPP, P1COOH and the three β-CD/PS systems ($\lambda_{exc.}$ = 419 nm). (A) Absorption spectra at a single concentration of DMSO and D_2O ([PS] = 4 μM) (the insert in the top right corner depicts the absorption spectra in DMSO), (B) fluorescence emission spectra, and (C) $^1O_2$ luminescence at a single concentration of D_2O (equal Soret bands at 0.2 ± 0.05 by dilution).

All these results indicate that both binding type between β-CD and PS can help to improve disaggregation of PSs in aqueous medium (*i.e.* $(β\text{-CD})_2$/*m*THPP inclusion complex and β-CD-P1 conjugate in monomeric forms in D_2O). In the case of non-covalent link, it should be noted that the improvement in disaggregation can be hampered by self-aggregation of the inclusion complex itself (*i.e.* $[(β\text{-CD})/\text{P1COOH}]_4$ inclusion complex).

3.6. Binding type effect on in vitro PDT efficacy of PSs

The binding type effect of β-CD on the *in vitro* PDT efficacy of PSs is investigated by comparing the *in vitro* dark cytotoxicity and phototoxicity of the free PSs and β-CD/PS systems at different PS concentrations (1, 2 and 3 μM) using human glioblastoma U87 cancer cells. After 24 h of incubation at 37

°C in the dark or after PDT treatment (652 nm, 10 J/cm^2, 36 min), cell viability is determined by the MTT assay as previously described [27]. The results of *in vitro* dark cytotoxicity and phototoxicity assays are presented in Fig. 9. It is worth noting that β-CD alone displays no dark cytotoxicity and phototoxicity on U87 cells within the concentration range used (from 1 to 3 µM). The dark cytotoxicity of free PSs on U87 cells (Figs. 9A and 9B) reveals a higher dark cytotoxic effect for *m*THPP than P1COOH suggesting that U87 cells are more sensitive to *m*THPP. As regards the comparison between *m*THPP and solid (β-CD)$_2$/*m*THPP inclusion complex, Fig. 9A indicates that inclusion complex reduces the dark cytotoxicity of *m*THPP, which could be explained by the fact that the inclusion of PS into β-CD host cavity limits direct contact between cells and PS, helping to reduce the dark cytotoxicity of *m*THPP. The opposite result obtained for P1COOH and solid [(β-CD)/P1COOH]$_4$ inclusion complex (*i.e.* inclusion complex more dark cytotoxic) could be explained by the high J-type self-aggregation of the inclusion complex in tetrameric form (see Sections 3.4. and 3.5.). With regard to the higher phototoxicity of free PSs relative to their inclusion complexes (Figs. 9A and 9B), a possible explanation is that the entrapment of the PS into the host cavity of β-CD reduces direct contact between cells and PS or at least reduces the time required for this interaction to occur, as recently suggested by T. A. Reis et al. [43]. Finally, comparative dark cytotoxicity and phototoxicity data for free P1COOH and β-CD-P1 conjugate (Fig. 9C) show that β-CD-P1 conjugate has the best *in vitro* PDT efficacy against glioblastoma U87 cells among the three β-CD/PS systems studied. The covalent conjugation of P1COOH to β-CD through a triazole link avoids aggregation compared to the solid [(β-CD)/P1COOH]$_4$ inclusion complex (see Sections 3.4. and 3.5.), leading to no dark cytotoxic effect and better PDT efficiency of β-CD-P1 conjugate on U87 cells (cell viability of 9 % at 3 µM). The *in vitro* PDT effectiveness of β-CD-P1 conjugate (from 1 to 20 µM) is also evidenced on human glioblastoma U251 cells resulting in no dark cytotoxicity and high phototoxicity (cell viability of 3 % at 3 µM, see Supporting Information, Fig. S6).

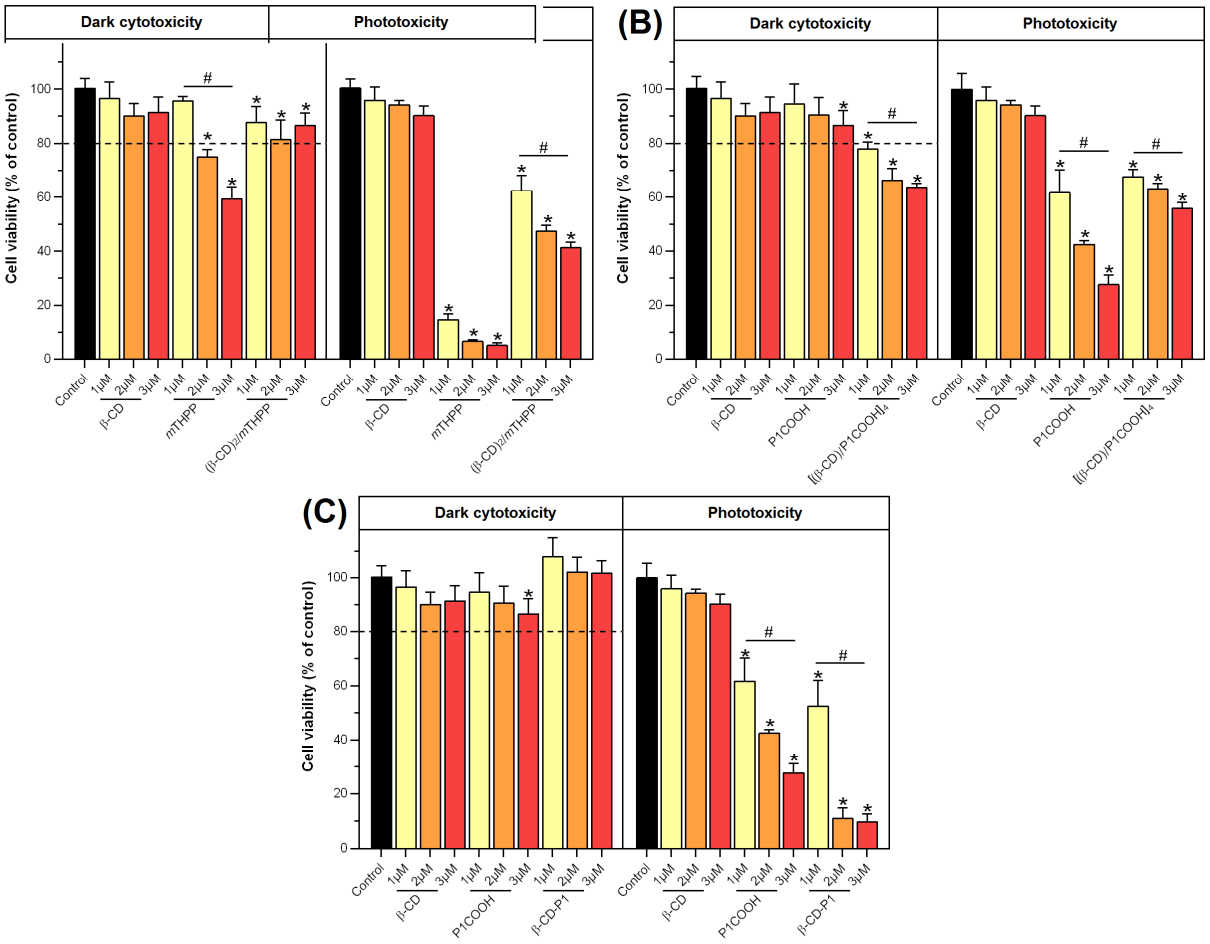

Fig. 9. Cell viability of U87 cells treated with (A) $(\beta\text{-CD})_2$/*m*THPP, (B) $[(\beta\text{-CD})/\text{P1COOH}]_4$ and (C) β-CD-P1 at PS concentration of 1-3 μM incubated into the dark (left, dark cytotoxicity) or after irradiation using a diode laser at a wavelength of 652 nm at a fluence of 10 J/cm^2 during 36 min (right, phototoxicity). Results were expressed as percentage of values obtained from untreated cells and given by mean ± SD, n = 3, $p \leq 0.05$. * *Vs.* control cells. # *Vs.* same compound at smaller concentration.

4. Conclusions

Three new β-CD/PS systems (*i.e.* solid $(\beta\text{-CD})_2$/*m*THPP and $[(\beta\text{-CD})/\text{P1COOH}]_4$ inclusion complexes and β-CD-P1 conjugate) are successfully synthesized *via* two different binding types (*i.e.* non-covalent and covalent) between β-CD and hydrophobic PS. The binding type effect and effectiveness on the disaggregation in aqueous medium and *in vitro* PDT efficacy against glioblastoma cancer cells of PSs are investigated.

The findings indicate that both binding type between β-CD and PS lead to an improvement of PSs disaggregation in aqueous medium but for the non-covalent binding type, this improvement could be hampered by self-aggregation of the inclusion complex itself. In addition, *in vitro* PDT activity against human glioblastoma cells reveals a higher *in vitro* PDT efficacy when the covalent binding type is used. As answer to our above hypothesis, the disaggregation in aqueous medium and *in vitro* anticancer PDT activity of hydrophobic PSs can be improved by their binding to β-CD and the covalent binding type is the most effective approach.

Authors contributions

This work was designed and supervised by S.A. The synthesis and characterization (FTIR, TG, DTA, powder XRD, NMR…) of the three β-CD/PS systems were conducted by A.B.M with the advice and assistance of L.C. The photophysical analyses (UV-vis, florescence and $^1O_2$ luminescence) were supervised by P.A. and C.F. *In vitro* studies were performed by Z.Y. and V.J.H. The draft manuscript was co-written by S.A., A.B.M. and R.V. All authors have given approval to the final version of the manuscript.

Declaration of Competing Interest

The authors declare no competing financial interest.

Acknowledgements

A.B.M. is supported by the Algerian Ministry of Higher Education and Scientific Research scholarship (No: 115/PNE: 2016/2017). The authors acknowledge Mathilde Achard for performing Mass experiments and Olivier Favre for running NMR experiments.

References

[1] Ackroyd, R., Kelty, C., Brown, N., and Reed, M. (2001). The history of photodetection and photodynamic therapy. *Photochemistry and Photobiology, 74*, 656–669. https://doi.org/10.1562/0031-8655(2001)0740656THOPAP2.0.CO2.

[2] Josefsen, L. B., and Boyle, R. W. (2012). Unique diagnostic and therapeutic roles of porphyrins and phthalocyanines in photodynamic therapy, imaging and theranostics. *Theranostics, 2*, 916–966. https://doi.org/10.7150/thno.4571.

[3] Staggers, N., McCasky, T., Brazelton, N., and Kennedy, R. (2008). Nanotechnology: The coming revolution and its implications for consumers, clinicians, and informatics. *Nursing Outlook, 56*, 268–274. https://doi.org/10.1016/j.outlook.2008.06.004.

[4] Marchal, S., El Hor, A., Millard, M., Gillon, V., and Bezdetnaya, L. (2015). Anticancer drug delivery: An update on clinically applied nanotherapeutics. *Drugs, 75*, 1601–1611. https://doi.org/10.1007/s40265-015-0453-3.

[5] Reshetov, V., Lassalle, H. P., Francois, A., Dumas, D., Hupont, S., Gräfe, S., Filipe, V., Jiskoot, W., Guillemin, F., Zorin, V., and Bezdetnaya, L. (2013). Photodynamic therapy with conventional and PEGylated liposomal formulations of mTHPC (temoporfin): Comparison of treatment efficacy and distribution characteristics *in vivo*. *International Journal of Nanomedicine, 8*, 3817–3831. https://doi.org/10.2147/IJN.S51002.

[6] Ogawara, K.-i., Shiraishi, T., Araki, T., Watanabe, T.-i., Ono, T., and Higaki, K. (2016). Efficient anti-tumor effect of photodynamic treatment with polymeric nanoparticles composed of polyethylene glycol and polylactic acid block copolymer encapsulating hydrophobic porphyrin derivative. *European Journal of Pharmaceutical Sciences, 82*, 154–160. https://doi.org/10.1016/j.ejps.2015.11.016.

[7] Kryjewski, M., Goslinski, T., and Mielcarek, J. (2015). Functionality stored in the structures of cyclodextrin–porphyrinoid systems. *Coordination Chemistry Reviews, 300*, 101–120. https://doi.org/10.1016/j.ccr.2015.04.009.

[8] Mazzaglia, A. (2011). Photodynamic tumor therapy with cyclodextrin nanoassemblies. Cyclodextrins in Pharmaceutics, Cosmetics, and Biomedicine (Bilensoy, E., Ed.) pp 343–361, Chapter 18, John Wiley & Sons, Inc., Hoboken. https://doi.org/10.1002/9780470926819.ch18.

[9] Cheirsilp, B., and Rakmai, J. (2016). Inclusion complex formation of cyclodextrin with its guest and their applications. *Biology, Engineering and Medicine, 2*, 1–6. https://doi.org/10.15761/BEM.1000108.

[10] Das, S. K., Rajabalaya, R., David, S., Gani, N., Khanam, J., and Nanda, A. (2013). Cyclodextrins-The molecular container. *Research Journal of Pharmaceutical, Biological and Chemical Sciences, 4*, 1694–172. ISSN: 0975-8585

[11] Dodziuk, H. (2006). Molecules with holes-cyclodextrins. Cyclodextrins and Their Complexes: Chemistry, Analytical Methods, Applications (Dodziuk, H., Ed.) pp. 1–30, Chapter 1, Wiley-VCH Verlag GmbH & Co. KGaA, Weinheim. https://doi.org/10.1002/3527608982.ch1.

[12] Patil, J. S., Kadam, D. V., Marapur, S. C., and Kamalapur, M. V. (2010). Inclusion complex system; a novel technique to improve the solubility and bioavailability of poorly soluble drugs: A review. *International Journal of Pharmaceutical Sciences Review and Research, 2*, 29–34.

[13] Zarzycki, P. K., Fenert, B., and Głód, B. K. (2016). Cyclodextrins-based nanocomplexes for encapsulation of bioactive compounds in food, cosmetics, and pharmaceutical products: Principles of supramolecular complexes formation, their influence on the antioxidative properties of target chemicals, and recent advances in selected industrial applications. Encapsulations: Nanotechnology in the Agri-Food Industry Volume 2 (Grumezescu, A. M., Ed.) pp. 717–767, Chapter 17, Academic Press, Cambridge. https://doi.org/10.1016/B978-0-12-804307-3.00017-X.

[14] Iacovino, R., Caso, J. V., Donato, C. D., Malgieri, G., Palmieri, M., Russo, L., and Isernia, C. (2017). Cyclodextrins as complexing agents: Preparation and applications. *Current Organic Chemistry, 21*, 162–176. https://doi.org/10.2174/1385272820666160909111842.

[15] Conte, C., Scala, A., Siracusano, G., Sortino, G., Pennisi, R., Piperno, A., Miro, A., Ungaro, F., Sciortino, M. T., Quaglia, F. et al. (2016). Nanoassemblies based on non-ionic amphiphilic cyclodextrin hosting Zn(II)-phthalocyanine and docetaxel: Design, physicochemical properties and intracellular effects. *Colloids and Surfaces B: Biointerfaces, 146*, 590–597. https://doi.org/10.1016/j.colsurfb.2016.06.047.

[16] Kirejev, V., Goncalves, A. R., Aggelidou, C., Manet, I., Martensson, J., Yannakopoulou, K., and Ericson, M. B. (2014). Photophysics and *ex vivo* biodistribution of beta-cyclodextrin-meso-tetra(m-hydroxyphenyl)porphyrin conjugate for biomedical applications. *Photochemical & Photobiological Sciences, 13*, 1185–1191. https://doi.org/10.1039/C4PP00088A.

[17] Mazzaglia, A., Sciortino, M. T., Kandoth, N., and Sortino, S. (2012). Cyclodextrin-based nanoconstructs for photoactivated therapies. *Journal of Drug Delivery Science and Technology, 22*, 235–242. https://doi.org/10.1016/S1773-2247(12)50034-1.

[18] Yankovsky, I., Bastien, E., Yakavets, I., Khludeyev, I., Lassalle, H. P., Gräfe, S., Bezdetnaya, L., and Zorin, V. (2016). Inclusion complexation with beta-cyclodextrin derivatives alters photodynamic activity and biodistribution of meta-tetra(hydroxyphenyl)chlorin. *European Journal of Pharmaceutical Sciences, 91*, 172–182. https://doi.org/10.1016/j.ejps.2016.06.012.

[19] Ben Mihoub, A., Larue, L., Moussaron, A., Youssef, Z., Colombeau, L., Baros, F., Frochot, C., Vanderesse, R., and Acherar, S. (2018). Use of cyclodextrins in anticancer photodynamic therapy treatment. *Molecules, 23*, 1936. https://doi.org/10.3390/molecules23081936.

[20] Job, P. (1928). Formation and stability of inorganic complexes in solution. *Annali di Chimica Applicata, 9*, 113–203.

583 [21] Catena, G. C., and Bright, F. V. (1989). Thermodynamic study on the effects of beta-cyclodextrin
584 inclusion with anilinonaphthalenesulfonates. *Analytical Chemistry, 61*, 905–909.
585 https://doi.org/10.1021/ac00183a024.
586 [22] Mohd Gazzali, A., Colombeau, L., Arnoux, P., Wahab, H. A., Frochot, C., Vanderesse, R., and
587 Acherar, S. (2017). Synthesis of mono-, di- and triporphyrin building blocks by click chemistry
588 for photodynamic therapy application. *Tetrahedron, 73*, 532–541.
589 https://doi.org/10.1016/j.tet.2016.12.037.
590 [23] Ben Mihoub, A., Saidat, B., Bal, Y., Frochot, C., Vanderesse, R., and Acherar, S. (2018).
591 Development of new ionic gelation strategy: Towards the preparation of new monodisperse and
592 stable hyaluronic acid/b-cyclodextrin-grafted chitosan nanoparticles as drug delivery carriers for
593 doxorubicin. *Frontiers of Materials Science, 12*, 83–94. https://doi.org/10.1007/s11706-018-
594 0407-2.
595 [24] Xu, M., Wu, S., Zeng, F., and Yu, C. (2010). Cyclodextrin supramolecular complex as a water-
596 soluble ratiometric sensor for ferric ion sensing. *Langmuir, 26*, 4529–4534.
597 https://doi.org/10.1021/la9033244.
598 [25] Seybold, P. G., and Gouterman, M. (1969). Porphyrins: XIII: Fluorescence spectra and quantum
599 yields. *Journal of Molecular Spectroscopy, 31*, 1–13. https://doi.org/10.1016/0022-
600 2852(69)90335-X.
601 [26] Wilkinson, F., Helman, W. P., and Ross, A. B. (1993). Quantum yields for the photosensitized
602 formation of the lowest electronically excited singlet oxygen state of molecular oxygen in
603 solution. *Journal of Physical and Chemical Reference Data, 22*, 113–262.
604 https://doi.org/10.1063/1.555934.
605 [27] Pramual, S., Lirdprapamongkol, K., Svasti, J., Bergkvist, M., Jouan-Hureaux, V., Arnoux, P.,
606 Frochot, C., Barberi-Heyob, M., and Niamsiri, N. (2017). Polymer-lipid-PEG hybrid
607 nanoparticles as photosensitizer carrier for photodynamic therapy. *Journal of Photochemistry and*
608 *Photobiology B: Biology B, 173*, 12–22. https://doi.org/10.1016/j.jphotobiol.2017.05.028.
609 [28] Bonnett, R. (2000). Photobleaching. Chemical Aspects of Photodynamic Therapy Volume 1
610 (Phillips, D., O'Brien, P., and Roberts, S., Eds.) pp 237–256, Chapter 12, Gordon and Breach
611 Science Publishers, London. https://doi.org/10.1201/9781482296952.
612 [29] Hunter, C. A., and Sanders, M. K. J. (1990). The nature of π-π interactions. *Journal of the*
613 *American Chemical Society, 112*, 5525–5534. https://doi.org/10.1021/ja00170a016.
614 [30] Siggel, U., Bindig, U., Endisch, C., Komatsu, T., Tsuchida, E., Voigt, E., and Fuhrhop, J. H.
615 (1996). Photophysical and photochemical properties of porphyrin aggregates. *Berichte der*

Bunsengesellschaft für Physikalische Chemie, 100, 2070–2075. https://doi.org/10.1002/bbpc.19961001225.

[31] Aggelidou, C., Theodossiou, T. A., and Yannakopoulou, K. (2013). Protoporphyrin IX–β-cyclodextrin bimodal conjugate: Nanosized drug transporter and potent phototoxin. *Photochemistry and Photobiology, 89*, 1011–1019. https://doi.org/10.1111/php.12127.

[32] Tau, P., Ogunsipe, A. O., Maree, S., Maree, M. D., and Nyokong, T. (2003). Influence of cyclodextrins on the fluorescence, photostability and singlet oxygen quantum yields of zinc phthalocyanine and naphthalocyanine complexes. *Journal of Porphyrins and Phthalocyanines, 7*, 439–446. https://doi.org/10.1142/S1088424603000562.

[33] Schneider, H.-J., Hacket, F., Rüdiger, V., and Ikeda, H. (1998). NMR studies of cyclodextrins and cyclodextrin complexes. *Chemical Reviews, 98*, 1755–1786. https://doi.org/10.1021/cr970019t.

[34] Answer, M. K., Jamil, S., Ansari, M. J., Al-Shdefat, R., Ali, B. E., Ganaie, M. A., Abdel-Kader, M. S., and Shakeel, F. (2014). Water soluble binary and ternary complexes of diosmin with β-cyclodextrin: Spectroscopic characterization, release studies and anti-oxidant activity. *Journal of Molecular Liquids, 199*, 35–41. https://doi.org/10.1016/j.molliq.2014.08.012.

[35] Gao, S., Liu, Y., Jiang, J., Ji, Q., Zhao, L., Li, C., and Ye, F. (2019). Physicochemical properties and fungicidal activity of inclusion complexes of fungicide chlorothalonil with β-cyclodextrin and hydroxypropyl-β-cyclodextrin. *Journal of Molecular Liquids, 293*, 111513. https://doi.org/10.1016/j.molliq.2019.111513.

[36] Ahmed, S. M., Naggi, A., Guerrini, M., and Focher, B. (1991). Inclusion complexes of bioprimine with β-Cyclodextrin in solution and in solid state. *International Journal of Pharmaceutics, 77*, 247–254. https://doi.org/10.1016/0378-5173(91)90323-G.

[37] Mura, P. (2015). Analytical techniques for characterization of cyclodextrin complexes in the solid state: A review. *Journal of Pharmaceutical and Biomedical Analysis, 113*, 226–238. https://doi.org/10.1016/j.jpba.2015.01.058.

[38] Zarif, M.S., Afidah, A. R., Abdullah, J. M., and Shariza, A. R. (2012). Physicochemical characterization of vancomycin and its complexes with β-cyclodextrin. *Biomedical Research (India), 23*, 513–520.

[39] Sapte, S., and Pore, Y. (2016). Inclusion complexes of cefuroxime axetil with β-cyclodextrin: Physicochemical characterization, molecular modeling and effect of L-arginine on complexation. *Journal of Pharmaceutical Analysis, 6*, 300–306. https://doi.org/10.1016/j.jpha.2016.03.004.

[40] Birks, J. B. (1970). Photophysics of aromatic molecules, Wiley-Interscience, London, https://doi.org/10.1002/bbpc.19700741223.

[41] Sameena, Y., Sudha, N., Chandrasekaran, S., and Enoch, I. V. M. V. (2014). The role of encapsulation by β-cyclodextrin in the interaction of raloxifene with macromolecular targets: a study by spectroscopy and molecular modeling. *Journal of Biological Physics, 40*, 347–367. https://doi.org/10.1007/s10867-014-9355-y

[42] Kano, K., Takei, M., and Hashimoto, S. (1990). Cationic porphyrins in water: proton NMR and fluorescence studies on dimer and molecular complex formation. *Journal of Physical Chemistry,* 94, 2181–2187. https://doi.org/10.1021/j100368a082.

[43] Reis, T. A., Jaculi, A. E., Ramos, K. L. V., Souza, P. E. N., Veiga-Souza, F. H., Joanitti, G. A., Azevedo, R. B., Gratieri, T., Cunha-Filho, M., and Gelfuso, G. M. (2019). Combination of cyclodextrin complexation and iontophoresis as a promising strategy for the cutaneous delivery of aluminum-chloride phthalocyanine in photodynamic therapy. *European Journal of Pharmaceutical Sciences, 139*, 105056. https://doi.org/10.1016/j.ejps.2019.105056.

Graphical Abstract (dimension 13 cm x 5 cm)